AGU PUBLICATIONS

Geophysical Research Letters

RESEARCH LETTER
10.1002/2015GL064256

Key Points:
- New method used for first separation of leakage components in a realistic hindcast
- Non-eddy flux is significant, and its ratio with eddy flux is decadally variable
- Flux variability is tied to westerly wind strength, modulated by SAM phase

Correspondence to:
B. R. Loveday,
blo@pml.ac.uk

Citation:
Loveday, B. R., P. Penven, and C. J. C. Reason (2015), Southern Annular Mode and westerly-wind-driven changes in Indian-Atlantic exchange mechanisms, *Geophys. Res. Lett.*, *42*, doi:10.1002/2015GL064256.

Received 15 APR 2015
Accepted 28 MAY 2015
Accepted article online 3 JUN 2015

Southern Annular Mode and westerly-wind-driven changes in Indian-Atlantic exchange mechanisms

B. R. Loveday[1,2], P. Penven[3], and C. J. C. Reason[1]

[1]Department of Oceanography, University of Cape Town, Cape Town, South Africa, [2]Egagasini Node, SAEON, Cape Town, South Africa, [3]LMI-ICEMASA, Laboratoire de Physique des Oceans, UMR 6523 (CNRS, IFREMER, IRD, UBO), Brest, France

Abstract The dynamical link between the Indian Ocean and Atlantic Meridional Overturning Circulation (AMOC) remains poorly understood. This partly arises from the complex Agulhas leakage, which occurs via rings, cyclones, and non-eddy flux. Hindcast simulations suggest that leakage has recently increased but have not decomposed this signal into its constituent mechanisms. Here these are isolated in a realistic ocean model. Increases in simulated leakage are attributed to stronger eddy and non-eddy-driven transports, and a strong warming and salinification, especially within Agulhas rings. Variability in both regimes is associated with strengthening Indian Ocean westerly winds, reflecting an increasingly positive Southern Annular Mode. While eddy and non-eddy flux signals are tied through turbulent eddy dissipation, the ratio between the two varies decadally. Consequently, while altimetry suggests a recent increase in retroflection turbulence and implied leakage, non-eddy flux may also play a significant role in modulating the leakage AMOC connection.

1. Introduction

At the southern tip of Africa, the Agulhas Current retroflects, returning most of its flux to the Indian Ocean via the Agulhas Return Current. Barring small fluxes across the Subtropical Front, the remainder of the incoming western boundary flux emanates from the retroflection as the Agulhas leakage, entering the South Atlantic Ocean via the turbulent Cape Basin. Consequently, the leakage represents the thermocline link between the Indian Ocean and Atlantic Ocean and plays a key role in determining global climate [*Beal et al.*, 2011]. While its variability may effect Atlantic Meridional Overturning Circulation (AMOC) strength [*Weijer et al.*, 2002] and glacial timing [*Bard and Rickaby*, 2009; *Peeters et al.*, 2004], this influence can depend on its distribution [*Weijer et al.*, 2002] and form [*Biastoch et al.*, 2008a].

Multiple mechanisms contribute to the total leakage: Agulhas rings, cyclones, filaments, coastal jets, and direct flux [*de Ruijter et al.*, 1999; *Gordon*, 1986]. Agulhas rings often split into smaller anticyclonic and cyclonic features [*Dencausse et al.*, 2010], contributing to a highly variable, eddy-rich system. Directly observing and quantifying these, often intermittent, turbulent mechanisms are challenging, and consequently, it is necessary to study the region with high-resolution ocean models.

In response to continued anthropogenic influence, the Southern Hemisphere westerly winds are increasing in intensity and migrating poleward, producing an increasingly positive phase of the Southern Annular Mode (SAM) [*Cai*, 2006]. Hindcast simulations suggest that, as a result, there has been a recent and substantial increase in Agulhas leakage [*Biastoch et al.*, 2009; *Rouault et al.*, 2009].

In this study, we use a high-resolution, multidecadal, hindcast simulation to relate the interdecadal variability of the Agulhas leakage to changes in the regional Indian Ocean winds and the phase of the SAM. After validating the performance of the simulation against altimetry, we decompose total leakage flux into anticyclonic, cyclonic, and non-eddy-driven contributions, allowing us to investigate changes in leakage structure over time. We hypothesize that increases in leakage flux, driven by strengthening westerly winds, are modulated by decadal variability in the SAM, which more strongly affects the non-eddy-driven component of the flux.

2. Methods

To assess the variability in the structure of the leakage, we compare the results of a regional ocean model of the greater Agulhas Region, ARC112i, with gridded altimetry products. ARC112i is a 1/12° eddy-resolving configuration, constructed using the Regional Ocean Modeling System (ROMS) [*Shchepetkin and McWilliams*,

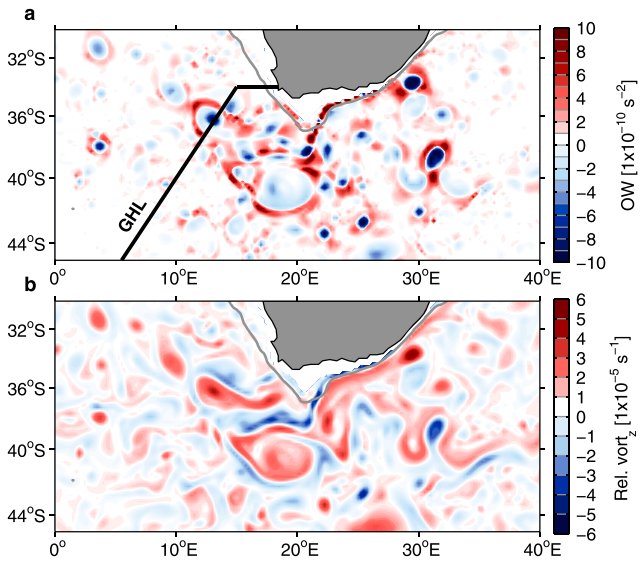

Figure 1. (a) Okubo-Weiss (OW) parameter derived from the 5-daily averaged model fields at 100 m, measured in s^{-2}. The black GHL transect represents the GoodHope Line. Where OW $< -2 \times 10^{-12} s^{-2}$, flow is determined to be eddy driven [*Chelton et al.*, 2007]. (b) The vertical component of relative vorticity, measured in s^{-1}, for the same depth and period. Here a horizontal depth slice is shown for clarity, but OW and relative vorticity are determined on the native model grid when calculating flux components. Flux across the GHL transect inshore of the 1000 m isobath (denoted by the grey contour) is recorded as a coastal flow component.

2005] that appropriately represents the Agulhas system (for a full model description, see *Loveday et al.* [2014]). At the surface, ARC112i is forced with daily radiation, fresh-water and momentum fluxes derived from version two of the corrected Coordinated Ocean-Ice Reference Experiments interannual forcing [*Large and Yeager*, 2004] (hereafter referred to as CORE v.2b), applied using the *Fairall et al.* [1996] bulk formulation. Monthly mean open boundary conditions are derived from a CORE v.2b forced, coarse resolution, ORCA05 global hindcast [*Biastoch et al.*, 2008b]. The ARC112i hindcast simulation extends from 1948 to 2007, with prognostic fields available as 5-daily averages throughout.

Surface mean (MKE) and eddy (EKE) kinetic energy fields are calculated from the zonal (u) and meridional (v) components of the geostrophic velocities, derived from hindcast sea surface height (SSH), and the combined gridded mean sea level anomaly and Rio09 [*Rio et al.*, 2009] mean dynamic topography obtained from Aviso. Velocities are determined from SSH by $u = -gf^{-1}\eta_y$ and $v = gf^{-1}\eta_x$, where g is gravity, f the Coriolis parameter, and η is SSH. MKE and EKE are calculated according to $(u'^2+v'^2)/2$ and $(\bar{u}^2+\bar{v}^2)/2$, respectively, where $u' = u-\bar{u}$ and $v' = v-\bar{v}$, where $\bar{u}$ and $\bar{v}$ are the centered annual running mean at each time step. Decadal trends are calculated using a least squares linear fit that minimizes the associated error.

Leakage flux components are determined according to an Okubo-Weiss parameter, $O_w = S_n^2+S_s^2-\xi^2$, where S_n and S_s are the normal $(\partial u/\partial x-\partial v/\partial y)$ and shear $(\partial v/\partial x+\partial u/\partial y)$ terms of the strain tensor, respectively, and ξ is the vertical component of relative vorticity $(\partial v/\partial x-\partial u/\partial y)$. Where $O_w < \varepsilon$, here set to $-2\times10^{-12}s^{-2}$, eddies dominate flow [*Chelton et al.*, 2007] (Figure 1a). The polarity of ξ is used to label cyclonic and anticyclonic eddies and produce four-dimensional *(x,y,z,t)* masks for anticyclonic ($O_w \le \varepsilon$; $\zeta_z > 0$) and cyclonic ($O_w \le \varepsilon$; $\zeta_z < 0$) flow (Figure 1b). A non-eddy flow mask is defined where $O_w \ge \varepsilon$. A fourth coastal component is defined as the net northward transport of Indian Ocean waters inshore of the 1000 m isobath.

The model includes a passive tracer, which labels Indian Ocean water masses. The tracer is nudged to 0 and 1 west of 20°W and east of 70°E, respectively. Between these longitudes the tracer evolves with the model advection and diffusion schemes. Volume fluxes for the leakage components are determined from the 5-daily averaged velocities, passive tracer concentration, and relevant mask values, integrated along the GoodHope Line (GHL) transect using the PAGO Eulerian transport package (http://www.whoi.edu/science/PO/pago).

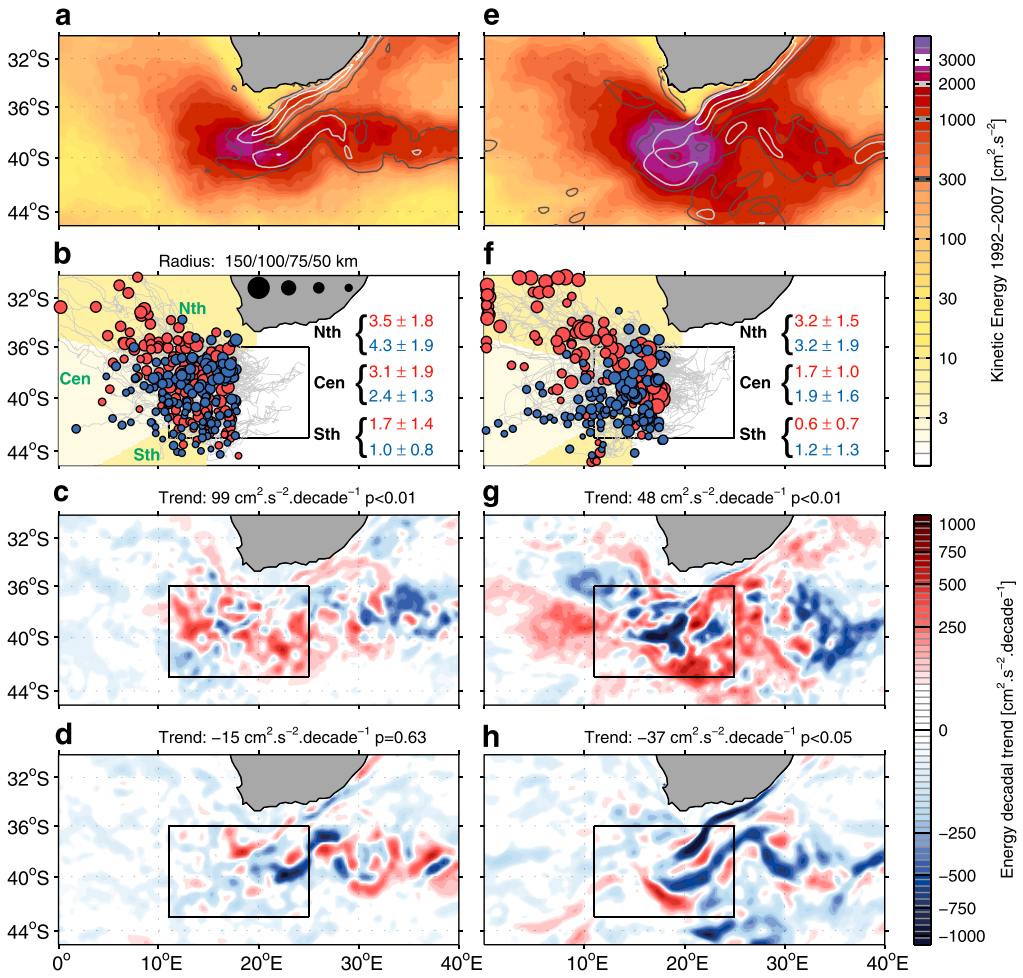

Figure 2. (a) Surface mean (contoured) and eddy (shaded) kinetic energy components, in $cm^2\ s^{-2}$, calculated from absolute geostrophic velocities derived from weekly altimetry for 1992 to 2007. (b) Altimetry-derived trajectories and final locations of long-lived (>2 months) cyclonic and anticyclonic eddies, shown, respectively, as blue and red dots, formed at the retroflection and persisting west of 18°E. Dot size scales with eddy radius according to the key shown above Figure 2b. Annotated statistics show the annual mean and standard deviation of the number of eddies that traverse the marked Northern (Nth), Central (Cen), and Southern (Sth) zones, as identified by *Dencausse et al.* [2010]. (c and d) The decadal trends in observed eddy and mean kinetic energy at the Agulhas retroflection, in $cm^2\ s^{-2}\ decade^{-1}$, with the area-averaged trend across the retroflection (represented by the black box) annotated above the relevant panel. (e–h) The analogous variables derived from the 5-daily ARC112i SSH for the 1992–2007 hindcast period. All trends are calculated using a least squares polynomial fit that minimizes the squared error. Statistical significance is based on a two-tailed Spearman rank correlation coefficient, with 794 and 1150 degrees of freedom for the weekly altimetry and 5-daily simulated SSH fields, respectively.

The method is unable to separate flux solely due to Agulhas rings from the generalized anticyclonic flow. However, we assume that the high concentration of Indian Ocean waters within rings are likely to make them the dominant anticyclonic contributor.

Eddies are identified and tracked using an eddy detection scheme that uses a hybrid criterion based on Okubo-Weiss value and closed-contour SSH loops. This approach reduces the sensitivity of the detection method to the value of ϵ used [*J. Souza et al.*, 2011]. Frame-to-frame tracking of eddy trajectories is based on minimizing the generalized distance between the two eddy fields in parameter space [*Penven et al.*, 2005; *J. Souza et al.*, 2011]. Retroflection eddies are isolated according to the following criteria. First, they must be generated in a box spanning 11°E–25°E, 43°S–36°S (plotted in black on Figures 2b–2d). Second, only eddies with lifetimes longer than 2 months are considered. Third, eddies must persist west of 18°E at the end of their lifetime to be considered.

Unless otherwise stated, all correlations are calculated from detrended time series, averaged across 5 year increments (e.g., 1948–1952) and referred to as "5-yearly binned" throughout. Trends are calculated according to a least squares polynomial fit that minimizes the squared error against the data, and with a statistical significance derived from the two-tailed Spearman rank correlation coefficient with a stated degree of freedom in all cases. We assume that no significant relationship exists where $p > 0.1$.

3. Results and Discussion

The surface expression of turbulence in the greater Agulhas system can be assessed by separating the mean (MKE) and eddy (EKE) kinetic energies. Figure 2 shows the similarity between the altimetry-derived energy signals (Figure 2a) and those extracted from the ARC112i hindcast for the 1992 to 2007 period (Figure 2e). Strong EKE signals at the retroflection confirm that the model appropriately captures the mesoscale variability of the Agulhas retroflection. In addition, low EKE and high MKE along the eastern margin of Africa show that the model exhibits a coherent western boundary current, with no spurious upstream recirculation; a common problem in many ocean model simulations of the region. Agulhas rings, a dominant leakage mechanism, have been identified as taking one of three bathymetry-determined paths across the Cape Basin [*Dencausse et al.*, 2010]. Figure 2b shows the altimetry-derived polarity and trajectories of all eddies generated at the retroflection between 1992 and 2007. The annotated statistics show that the northern path (Nth) dominates, recording 3.5 ± 1.8 anticyclonic and 4.3 ± 1.9 cyclonic features per year, followed by the central path (Cen), and latterly the southern (Sth). An analogous assessment of the hindcast (Figure 2f) shows that the mean and standard deviation in eddy number in the northern path is consistent with those observed. In sigma coordinate models, it is necessary to smooth steep topography to reduce pressure gradient errors. This smoothing process reduces the vertical extent of isolated steep features, such as the Erica seamount. Consequently, the Erica seamount, which separates the northern (Nth) and central pathways, does not form as formidable barriers in the model as it does in reality and may contribute to the underestimation of eddies taking the central path in the model (1.7 ± 1.0 anticyclones per year versus the 3.1 ± 1.9 observed).

A recent intensification of Indian Ocean winds has driven an increase in the mesoscale variability of the greater Agulhas system [*Backeberg et al.*, 2012]. Between 1992 and 2007, trends in observed EKE (Figure 2c) across the retroflection show a statistically significant increase of 99 $cm^2\ s^{-2}\ decade^{-1}$ ($p < 0.01$), while MKE shows no trend as the $-16\ cm^2\ s^{-2}\ decade^{-1}$ decrease is statistically insignificant ($p = 0.63$) (Figure 2d). Simulated trends in EKE/MKE are intrinsically linked to the choice of surface forcing use, as different wind fields have been shown to vary in their representation of recent wind intensification [*Backeberg et al.*, 2012]. However, decadal trends derived from the CORE v.2b forced hindcast approximate those observed, recording statistically significant trends of $48\ cm^2\ s^{-2}\ decade^{-1}$ ($p < 0.01$) for EKE (Figure 2g) and $-37\ cm^2\ s^{-2}\ decade^{-1}$ ($p < 0.1$) for MKE (Figure 2h). Spatially, observations and simulation suggest a consistent decrease in western boundary MKE south of 32°S, which persists around the retroflection loop. Although simulated EKE patterns at 20°E deviate from observations, increases at western boundary and decreases in the return current downstream of 30°E are common to both patterns. In the Cape Basin, the observed EKE pattern, an increase adjacent to the shelf and at 40°S, separated by a band of decreasing variability, is echoed in the model.

Multidecadal intensification of the westerly winds has been linked with the depletion of Antarctic ozone, driven by anthropogenic forcing, and is reflected in an increasingly positive state of the Southern Annular Mode (SAM) [*Marshall*, 2003]. Comparing the observed normalized SAM index (Figure 3a; dark blue) with that expressed by the CORE v.2b forcing fields (Figure 3a; red) shows that the reanalysis product accurately recreates the observed signal ($r = 0.871, p < 0.01$). Both the observed ($r = 0.756, p < 0.01$) and reanalysis-derived ($r = 0.872, p < 0.01$) indices correlate strongly with the 5-yearly binned subtropical Indian Ocean wind stress curl (WSC), calculated as the average value over a box spanning 47°S–35°S, 20°E–115°E (Figure 3a; cyan trace), confirming the role that the SAM plays in the decadal modulation of the Indian Ocean westerly winds. Positive trends of $0.167\ decade^{-1}$ in the BAS SAM index ($r = 0.612, p < 0.05$), $0.389\ decade^{-1}$ in the CORE v.2b SAM index ($r = 0.965, p < 0.01$), and $0.057 \times 10^{-7}\ Nm^3\ decade^{-1}$ in the WSC, ($r = 0.923, p < 0.01$) are all highly significant with 12 degrees of freedom.

Annually binned time series of these Agulhas leakage components are shown in the bottom panel of Figure 3a. Drifter-based estimates of Agulhas leakage record an interbasin flux of at least 15 Sv (sverdrup: $1\ Sv = 1 \times 10^6\ m^3\ s^{-1}$) in the top 1000 m [*Richardson*, 2007], 20% lower than the full-depth total mean value of 18.9 Sv recorded by the hindcast (Figure 3a, black line). An independent Lagrangian assessment of the Agulhas

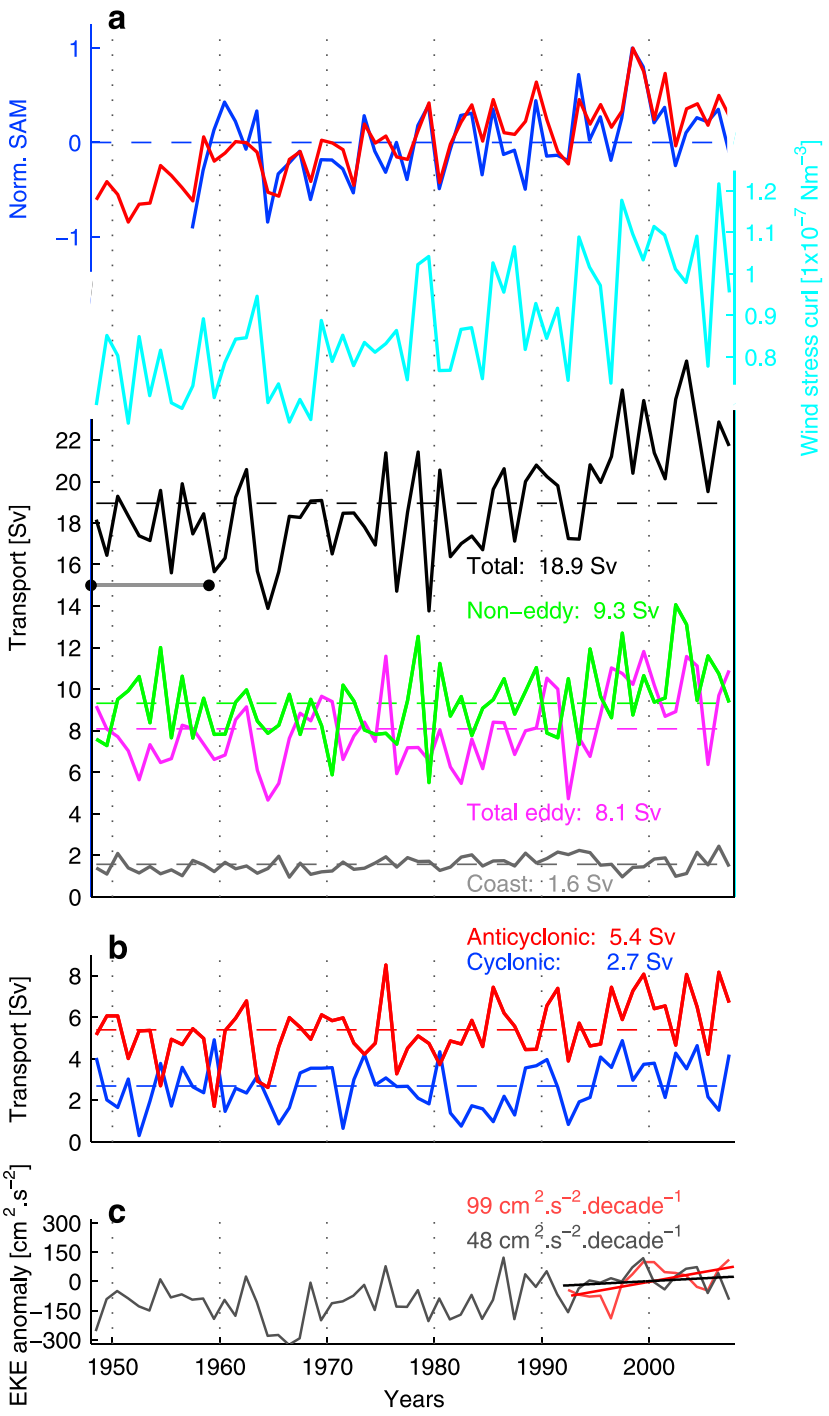

Figure 3. (a) Annually binned normalized Southern Annular Mode (SAM) indices derived from the BAS observations [*Marshall*, 2003], in blue and from the CORE v.2b [*Large and Yeager*, 2004] fields used to force the ARC112i hindcast, in red. The CORE v.2b SAM index is derived as per the method described in *Marshall* [2003]. The cyan line shows annually binned wind stress curl (in Nm^{-3}) averaged over a box spanning 20°E–115°E, 47°S–35°S, also extracted from the CORE v.2b reanalysis. Annually binned total Agulhas leakage transport in Sv (sverdrup: 1 Sv = 1×10^6 m^3 s^{-1}), shown in black, is separated into non-eddy (green), eddy (magenta), and coastal (grey) flux using the Okubo-Weiss parameter. An observed estimate of total Agulhas leakage above 1000 m is shown by the black bar [*Richardson*, 2007]. (b) Further division of the eddy-driven flux into anticyclonic and cyclonic contributions. (c) Annually binned EKE anomalies (in cm^2 s^{-2}) from the 1992–2007 mean value, averaged over the Agulhas retroflection box (Figure 1e) for the hindcast (dark grey) and altimetry (red). The decadal increase in the 1992–2007 period is noted by the trend line and annotation in the respective color.

leakage, which excludes diffusive processes, produced a near-identical mean leakage value [*Loveday et al.*, 2014], confirming the dominant role of turbulent advection. Consistent with previous hindcasts [*Biastoch et al.*, 2009; *Rouault et al.*, 2009], total simulated leakage increases substantially from the early 1980s. This increase is also evident in estimates of Agulhas leakage reconstructed from altimetry, when considering the common 1992–2007 period [*Le Bars et al.*, 2014].

Although recent hindcasts suggest that leakage increases are attributable to a southward migration in the zero line of wind stress curl [*Biastoch et al.*, 2009], idealized simulations suggest that it is rather the intensification of the Southern Hemisphere westerly winds that exerts the strongest influence [*Durgadoo et al.*, 2013]. Here this latter relationship is shown to hold on an interdecadal basis. The total leakage magnitude (Figure 3a; black trace) and WSC show a consistent pattern, correlating significantly ($r = 0.503$, $p < 0.1$), when binned into 5 year periods. While total leakage shows a consistent positive trend of 0.84 Sv decade^{-1} across the record ($r = 0.797$, $p < 0.01$), marked decreases in leakage around 1964, 1982, and 1992 are all associated with sharp reductions in westerly wind intensity and follow negative deviations in the SAM.

When separated, eddy, non-eddy, and coastal flux are shown to contribute to the total with a ratio of 4:5:1 in the mean (Figure 3a, bottom panel). Interannual variability in the coastal component remains low; however, there are pronounced modulations in the other fluxes. Periods of decreased eddy export occur prior to 1964 and from 1977 to 1987. During the latter period, the weakened eddy component is compensated by increased non-eddy flux, which shows a continuing increase in the post-1992 altimetry era. Contributions to the stronger Agulhas leakage after 1995 are equally attributable to the eddy and non-eddy components of the flux, with non-eddy flux taking an increasing role later after 2000. Eddy flux shows no statistical relation to either the 5-yearly binned Indian Ocean WSC or the CORE v.2b SAM index. However, non-eddy flux correlates with both WSC ($r = 0.576$, $p < 0.05$) and the SAM index ($r = 0.594$, $p = 0.07$). Revisiting the statistical relationship using a 10 year binned decadal time series leads to a more robust correlation of $r = 0.830$ ($p < 0.05$) between non-eddy flux and WSC, and $r = 0.898$ ($p < 0.01$) between non-eddy flux and the CORE v.2b derived SAM index.

Further decomposing the eddy component by polarity (Figure 3b) shows that anticyclonic features (rings and subrings) contribute around two thirds of the eddy flux, consistent with previous Lagrangian studies [*Doglioli et al.*, 2006; *Boebel et al.*, 2003]. Anticyclonic features contribute 5.4 Sv to the mean taken across the entire hindcast. A mean value of 6.7 Sv is recorded between 1998 and 2007, falling within the range of estimates derived from in situ observations during this period [*J. M. Souza et al.*, 2011; *Garzoli*, 1999] but less than that inferred from altimetry [*Dencausse et al.*, 2010], likely due to ambiguity in determining the vertical extent of the rings in the latter case. Cyclonic features, which form a substantial contribution to Cape Basin turbulence, contribute 2.5 Sv to mean total flux. Coevolution of the anticyclonic and cyclonic flux contributions suggest that the two are associated through the ring splitting and vigorous mixing [*Boebel et al.*, 2003]. Significant positive trends of 0.31 Sv decade^{-1} and 0.14 Sv decade^{-1} are evident in the respective anticyclonic ($r = 0.755$, $p < 0.01$) and cyclonic ($r = 0.573$, $p < 0.05$) components.

The global-scale supergyre links the midlatitude circulation of the South Pacific Ocean, South Indian Ocean, and South Atlantic Ocean [*Ridgeway and Dunn*, 2007]. During positive phases of the SAM, the westerly wind belt across the Indian Ocean contracts toward Antarctica, producing a positive anomaly in WSC across the Indian Ocean basin at the latitude of the retroflection. In response, meridional sverdrup transport across the southern branch of the supergyre increases [*Durgadoo et al.*, 2013], and the supergyre intensifies [*Cai et al.*, 2005]. Consequently, as continuity requires that the meridional mass transport must be balanced by westward transport in the northern branch of the supergyre, the Agulhas leakage is also enhanced [*Durgadoo et al.*, 2013; *Cai et al.*, 2005].

However, due to a high degree of nonlinearity in the Agulhas system, it is clear that local dynamics play a substantial role. A strong negative anomaly in total flux during the mid-1960s (Figure 3a), reflected in the eddy flux contribution, is also clearly linked to an eastward deviation in the retroflection position (Figure 4a). *Loveday et al.* [2014] show that the retroflection position is stable in the face of large changes in the inertia of the Agulhas Current. This deviation is assumed, therefore, to be a response to a cascade of upstream variability, as observed in the early retroflection of 2001 [*van Aken et al.*, 2013]. Irrespective of the change in eddy flux, non-eddy flux during the mid-1960s remains minimally affected. Consequently, while ring formation is governed by local nonlinear processes [*Pichevin et al.*, 1999], background flow appears to be governed by the linear wind-driven dynamics evident from the correlation between non-eddy flux and WSC.

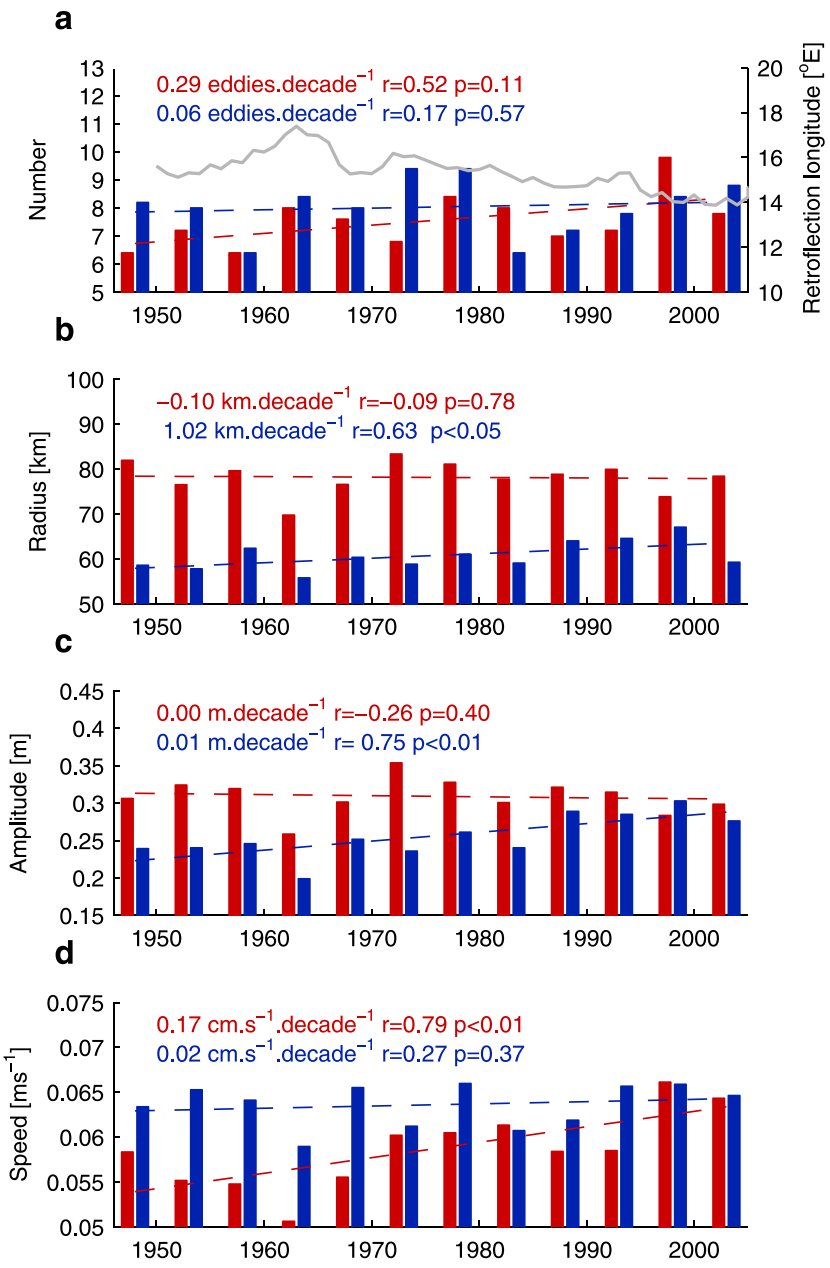

Figure 4. Five-yearly binned statistics of tracked eddies, showing (a) average number of eddies detected, (b) average eddy radius, (c) average eddy amplitude, and (d) average eddy speed. Anticyclones are denoted by red bars, cyclones by blue bars. Decadal trends are calculated using a least squares polynomial fit that minimizes the squared error, with statistical significance derived from the two-tailed Spearman rank correlation coefficient, with 12 degrees of freedom. The grey line overlaying Figure 4a shows the annual mean longitudinal position of the Agulhas retroflection loop, derived using the method described in *Loveday et al.* [2014] and *Backeberg et al.* [2012].

Idealized simulations show that changes in EKE do not necessarily correspond with changes in leakage [*Loveday et al.*, 2014; *Durgadoo et al.*, 2013]. Here 5-yearly binned retroflection EKE (Figure 3c) shows a positive trend of 29 cm^2 s^{-2} decade^{-1} ($r = 0.741$, $p < 0.01$) throughout the record and correlates strongly with total ($r = 0.786$, $p < 0.01$) and eddy flux ($r = 0.780$, $p < 0.01$), suggesting an increasingly turbulent retroflection and Cape Basin under intensified westerlies. There is, however, no direct correlation between simulated EKE and either the 5-yearly binned WSC or the CORE v.2b derived SAM index.

Figure 4 presents a census of eddy properties throughout the hindcast. From this it is clear that the strong increasing trend in leakage is not reflected in the number of eddies generated (Figure 4a). Rather, the

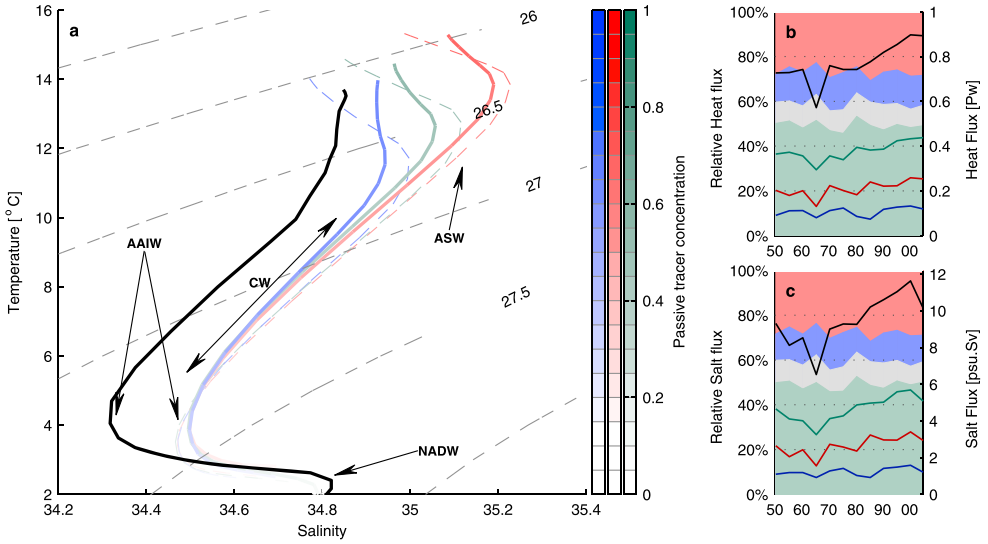

Figure 5. (a) Temperature-salinity diagram showing the distribution of mean water mass properties along the GHL transect. Trace properties are taken as averages along the transect at World Ocean Atlas (WOA09)-determined [*Antonov et al.*, 2010; *Locarnini et al.*, 2010] depth intervals for the 1968–1977 (dashed lines) and 1998–2007 (solid lines) periods, and separated according to flux component: anticyclonic (red), cyclonic (blue), and non-eddy (green). Line shading is scaled according to the passive tracer concentration, representing the percentage of Indian-Ocean-derived waters present. The heavy black line shows the mean water mass properties extracted from the WOA09 using the same method. Annotations represent North Atlantic Deep Water (NADW), Antarctic Intermediate Water (AAIW), Central Water (CW), and Agulhas Surface Water (ASW). (b and c) Shown, in shading, are the 5-yearly binned relative contributions that the anticyclonic (red), cyclonic (blue), non-eddy (green), and coastal (grey) components make to total heat and salt flux. The superimposed lines show the absolute fluxes in the relevant colors, with total flux in black. Fluxes are calculated using the mean salinity and temperature across the South Atlantic ocean between 25°W–0°W, 40°S–20°S as reference values.

positive trend in cyclonic flux is mirrored in cyclones of increasing radius (Figure 4b) and amplitude (Figure 4c). In parallel, trends in anticyclonic flux are associated with a notable increase in speed (Figure 4d). Idealized ring models [*de Steur*, 2004] suggest that faster ring advection should result in faster dissipation of their internal properties. Therefore, as stronger westerlies drive increased eddy speed, the rate at which the rings dissipate their signal into the non-eddying background should be enhanced, reflected in the strong correlation between total flux and EKE at the retroflection.

Interbasin volume flux is an important parameter for assessing Agulhas dynamics. However, changes in the export of heat and salt into the South Atlantic are highly relevant for AMOC variability [*Weijer et al.*, 2002] and South Atlantic sea surface temperature (SST) anomalies influence regional climate [*Reason and Jagadheesha*, 2005; *Hansingo and Reason*, 2009].

Figure 5 shows the change in the water masses between 1968–1977 and 1998–2007, as sampled across the GHL. Agulhas Surface waters (ASW), which originate in the Indian Ocean, are, as expected, much more pronounced in the anticyclonic regime, due to the action of Agulhas rings (Figure 5a, red line). By comparison, cyclones (blue line) retain much less of this Indian Ocean imprint, as they may form locally [*Penven et al.*, 2001]. The mixing of the eddy regimes with the surrounds results in non-eddy trace properties that lie between these two end points (green line). Comparing non-eddy water mass properties with those derived from WOA09 [*Antonov et al.*, 2010; *Locarnini et al.*, 2010] (Figure 5a, black line) suggests that the model has a salinity bias of 0.18, which extends into the intermediate layers. Near-zero passive tracer values in the simulated North Atlantic Deep Water (NADW) show that leakage is confined to the intermediate layers and shallower.

In the 1998–2007 decade, the subsurface salinity maximum associated with the ASW is substantially eroded; an effect most pronounced in the cyclonic field. This is coupled to a simultaneous and substantial increase in surface salinity, implying a possible increase in Ekman-driven mixing driven by increased wind stress. Below this, intermediate-depth central waters (CW), <50% of which are derived from the Indian Ocean, show a pervasive warming and freshening, consistent with an observed warming of the region [*Rouault et al.*, 2009]. In the intermediate waters, Antarctic Intermediate Waters (AAIW) become warmer and more saline in the later

decade. Comparing water mass properties between two decades gives an insight into discrete local changes, but it does not imply that these changes are monotonic or unidirectional. Both changes in the formation characteristics of these water masses and their advective route to the Agulhas system may vary on decadal time scales.

The cumulative effect of changes in volume flux and water mass properties is a substantial increase in total heat and salt flux across the GHL transect (Figures 5b and 5c, black lines), predominantly attributable to non-eddy (green lines) and anticyclonic (red lines) flux components. However, in relative terms, it is clear that, since 1965, the anticyclonic regime is playing an increasingly important role.

4. Conclusion

Using a realistic ocean model, we simulate a multidecadal increase in Agulhas leakage that is consistent with previous hindcasts [*Biastoch et al.*, 2009; *Rouault et al.*, 2009]. Building on previous idealized simulations [*Durgadoo et al.*, 2013], we have shown that this increase is attributable to the strengthening of the westerly winds across the Indian Ocean basin, moderated by decadal changes in the phase of the SAM. By separating leakage components we derive an anticyclonic flux estimate that is consistent with Agulhas ring observations [*J. M. Souza et al.*, 2011; *Garzoli*, 1999] and previous model studies [*Doglioli et al.*, 2006; *Boebel et al.*, 2003] but show that non-eddy flux plays a dominant role in Agulhas leakage transport. The results imply that leakage estimates based on the eddy field alone may underestimate total flux and challenge the assumption that leakage is ring dominated away from the retroflection. With stronger westerly winds and an increasingly positive SAM phasing projected [*Fyfe et al.*, 1999], Agulhas leakage seems likely to strengthen [*Biastoch and Böning*, 2013] and may partially ameliorate the AMOC slowdown predicted by coarse-resolution climate model projections [*Spooner et al.*, 2013]. Further, wider distribution and potentially increased retention of a South Atlantic warming signal is likely to have consequences for Southern African climate, a region that is highly sensitive to the SST in the adjacent basins [*Reason and Jagadheesha*, 2005; *Hansingo and Reason*, 2009].

Acknowledgments

The development of ARC112i and its analysis received funding from the European Community's Seventh Framework Programme FP7/2007-2013-Marie-Curie GATEWAYS ITN, the International Centre for Education, Marine and Atmospheric Sciences over Africa (ICE-MASA), and the UCT Marine Research Institute (MaRe). Simulations were performed at DST/CSIR CHPC in Cape Town. Please contact the corresponding author for use of published data. Altimetry products were produced by Ssalto/Duacs and distributed by Aviso, with support from CNES (www.aviso.oceanobs.com/duacs/). We thank J. Deshayes for providing, and helping to configure, the PAGO routines and J. Durgadoo for providing open boundary conditions.

The Editor thanks Bjorn Backeberg and an anonymous reviewer for their assistance in evaluating this paper.

References

Antonov, J., D. Seidov, T. Boyer, R. Locarnini, A. Mishonov, H. Garcia, O. Baranova, M. Zweng, and D. R. Johnson (2010), World Ocean Atlas 2009, Volume 2: Salinity, in *NOAA Atlas NESDIS 69*, edited by S. Levitus, 184 pp., U.S. Gov. Print. Off., Washington, D. C.

Backeberg, B. C., P. Penven, and M. Rouault (2012), Impact of intensified Indian Ocean winds on mesoscale variability in the Agulhas system, *Nat. Clim. Change*, *2*, 1–5.

Bard, E., and R. Rickaby (2009), Migration of the subtropical front as a modulator of glacial climate, *Nature*, *460*, 380–383.

Beal, L. M., W. de Ruijter, A. Biastoch, and R. Zahn (2011), On the role of the Agulhas system in ocean circulation and climate, *Nature*, *472*(7344), 429–36.

Biastoch, A., and C. Böning (2013), Anthropogenic impact on Agulhas leakage, *Geophys. Res. Lett.*, *40*, 1138–1143, doi:10.1002/grl.50243.

Biastoch, A., C. Böning, and J. Lutjeharms (2008a), Agulhas leakage dynamics affects decadal variability in Atlantic overturning circulation, *Nature*, *456*(7221), 489–492.

Biastoch, A., C. Böning, J. Getzlaff, J.-M. Molines, and G. Madec (2008b), Causes of interannual-decadal variability in the meridional overturning circulation of the mid-latitude North Atlantic Ocean, *J. Clim.*, *21*, 6599–6615.

Biastoch, A., C. Böning, F. U. Schwarzkopf, and J. Lutjeharms (2009), Increase in Agulhas leakage due to poleward shift of Southern Hemisphere westerlies, *Nature*, *462*(7272), 495–498.

Boebel, O., J. Lutjeharms, C. Schmid, W. Zenk, T. Rossby, and C. Barron (2003), The Cape Cauldron: A regime of turbulent inter-ocean exchange, *Deep Sea Res., Part II*, *50*, 57–86.

Cai, W. (2006), Antarctic ozone depletion causes an intensification of the Southern Ocean super-gyre circulation, *Geophys. Res. Lett.*, *33*, L03712, doi:10.1029/2005GL024911.

Cai, W., G. Shi, T. Cowan, D. Bi, and J. Ribbe (2005), The response of the Southern Annular Mode, the East Australian Current, and the southern mid-latitude ocean circulation to global warming, *Geophys. Res. Lett.*, *32*, L23706, doi:10.1029/2005GL024701.

Chelton, D., M. Schlax, R. Samelson, and R. Szoeke (2007), Global observations of large oceanic eddies, *Geophys. Res. Lett.*, *34*, L15606, doi:10.1029/2007GL030812.

Dencausse, G., M. Arhan, and S. Speich (2010), Routes of Agulhas rings in the southeastern Cape Basin, *Deep Sea Res., Part II*, *57*, 1406–1421.

Doglioli, A., M. Veneziani, B. Blanke, S. Speich, and A. Griffa (2006), A Lagrangian analysis of the Indian-Atlantic interocean exchange in a regional model, *Geophys. Res. Lett.*, *33*, L14611, doi:10.1029/2006GL026498.

Durgadoo, J. V., B. R. Loveday, C. J. C. Reason, P. Penven, and A. Biastoch (2013), Agulhas leakage predominantly responds to the Southern Hemisphere westerlies, *J. Phys. Oceanogr.*, *43*, 2113–2131.

de Ruijter, W., A. Biastoch, S. Drijfhout, J. Lutjeharms, R. Matano, T. Pichevin, P. Van Leeuwen, and W. Weijer (1999), Indian-Atlantic interocean exchange: Dynamics, estimation and impact, *J. Geophys. Res.*, *104*(9), 20,885–20,910.

de Steur, L. (2004), Tracer leakage from modeled Agulhas rings, *J. Phys. Oceanogr.*, *34*, 1387–1399.

Fairall, C. W., E. F. Bradley, D. P. Rogers, J. B. Edson, and G. S. Young (1996), Bulk parameterization of air-sea fluxes for tropical ocean-global atmosphere coupled-ocean atmosphere response experiment, *J. Geophys. Res.*, *101*(2), 3747–3764.

Fyfe, J. C., G. J. Boer, and G. M. Flato (1999), The Arctic and Antarctic Oscillations and their projected changes under global warming, *Geophys. Res. Lett.*, *26*(11), 1691–1604.

Garzoli, S. (1999), Three Agulhas rings observed during the Benguela Current experiment, *J. Geophys. Res.*, *104*(9), 20,971–20,985.

Gordon, A. (1986), Interocean exchange of thermocline water, *J. Geophys. Res.*, *91*(4), 5037–5046.

Hansingo, K., and C. J. C. Reason (2009), Modelling the atmospheric response over southern Africa to SST forcing in the southeast tropical Atlantic and southwest subtropical Indian oceans, *Int. J. Climatol.*, *29*(7), 1001–1012.
Large, W., and S. Yeager, (2004), Diurnal to decadal global forcing for oceans and sea-ice models: The data set and flux climatologies, *NCAR Tech. Note: NCAR/TN-460+STR*, Natl. Cent. for Atmos. Res., Boulder, Colo., pp. 1–112.
Le Bars, D., J. V. Durgadoo, H. A. Dijkstra, A. Biastoch, and W. de Ruijter (2014), An observed 20-year time series of Agulhas leakage, *Ocean Sci.*, *10*(4), 601–609.
Locarnini, R., A. Mishonov, J. Antonov, T. Boyer, H. Garcia, O. Baranova, M. Zweng, and D. R. Johnson (2010), World Ocean Atlas 2009, Volume 1: Temperature, in *NOAA Atlas NESDIS 68*, edited by S. Levitus, 184 pp., U.S. Gov. Print. Off., Washington, D. C.
Loveday, B. R., J. V. Durgadoo, C. J. C. Reason, A. Biastoch, and P. Penven (2014), Decoupling of the Agulhas leakage from the Agulhas current, *J. Phys. Oceanogr.*, *44*, 1776–1797.
Marshall, G. J. (2003), Trends in the Southern Annular Mode from observations and reanalyses, *J. Clim.*, *16*, 4134–4143.
Peeters, F., R. Acheson, G. Brummer, W. de Ruijter, R. Schneider, G. Ganssen, E. Ufkes, and D. Kroon (2004), Vigorous exchange between the Indian and Atlantic oceans at the end of the past five glacial periods, *Nature*, *430*, 661–665.
Penven, P., J. R. E. Lutjeharms, P. Marchesiello, C. Roy, and S. J. Weeks (2001), Generation of cyclonic eddies by the Agulhas Current in the lee of the Agulhas Bank, *J. Geophys. Res.*, *27*(6), 1055–1058.
Penven, P., V. Echevin, J. Pasepera, F. Colas, and J. Tam (2005), Average circulation, seasonal cycle, and mesoscale dynamics of the Peru Current System: A modeling approach, *J. Geophys. Res.*, *110*, C10021, doi:10.1029/2005JC002945.
Pichevin, T., D. Nof, and J. Lutjeharms (1999), Why are there Agulhas rings?, *J. Phys. Oceanogr.*, *29*(4), 693–707.
Reason, C. J. C., and D. Jagadheesha (2005), Relationships between South Atlantic SST variability and atmospheric circulation over the South African region during austral winter, *J. Clim.*, *18*(16), 3339–3355.
Richardson, P. (2007), Agulhas leakage into the Atlantic estimated with subsurface floats and surface drifters, *Deep Sea Res., Part I*, *54*(8), 1361–1389.
Ridgeway, K., and J. Dunn (2007), Observational evidence for a Southern Hemisphere oceanic supergyre, *Geophys. Res. Lett.*, *34*, L13612, doi:10.1029/2007GL030392.
Rio, M., P. Schaeffer, G. Moreaux, J.-M. Lemoine, and E. Bronner (2009), A new mean dynamic topography computed over the global ocean from grace data, altimetry and in situ measurments, paper presented at Poster Communication at OceanObs09 Symposium, Venice, 21–25 Sept.
Rouault, M., P. Penven, and B. Pohl (2009), Warming in the Agulhas Current system since the 1980's, *Geophys. Res. Lett.*, *36*, L12602, doi:10.1029/2009GL037987.
Shchepetkin, A., and J. McWilliams (2005), The regional oceanic modeling system (ROMS): A split-explicit, free-surface, topography-following-coordinate oceanic mode, *Ocean Modell.*, *9*, 347–404.
Souza, J., C. de Montegut, and P. Le Traon (2011), Comparison between three implementations of automatic identification algorithms for the qualification and characterization of mesoscale eddies in the South Atlantic Ocean, *Ocean Sci.*, *7*, 317–334.
Souza, J. M., C. de Boyer Montegut, C. Cabanes, and P. Klein (2011), Estimation of the Agulhas ring impacts on meridional heat fluxes and transport using Argo floats and satellite data, *Geophys. Res. Lett.*, *38*, L21602, doi:10.1029/2011GL049359.
Spooner, P. T., H. L. Johnson, and T. J. Woolings (2013), Influence of the Southern Annular Mode on projected weakening of the Atlantic Meridional Overturning Circulation, *J. Clim.*, *26*(20), 8017–8036.
van Aken, H. M., J. R. E. Lutjeharms, M. Rouault, C. Whittle, and W. de Ruijter (2013), Observations of an early Agulhas current retroflection event in 2001: A temporary cessation of inter-ocean exchange south of Africa?, *Deep Sea Res., Part I*, *72*, 1–8.
Weijer, W., W. de Ruijter, A. Sterl, and S. Drijfhout (2002), Response of the Atlantic overturning circulation to South Atlantic sources of buoyancy, *Global Planet. Change*, *34*(3–4), 293–311.